Electronic Supporting Information

Unveiling of Smartphone mediated 'ratiometric' ChromoSensor towards nanomolar level detection of lethal CN⁻: A combined experimental and theoretical validation with proposition of molecular Logic Circuitry

Suparna Paul,[a,b] Udayan Mondal,[a,b] Somrita Nag,[a,b] Madhupa Seth[c] and Priyabrata Banerjee[a,b]*

[a.] *Surface Engineering & Tribology Group, CSIR-Central Mechanical Engineering Research Institute, Mahatma Gandhi Avenue, Durgapur 713209, India. Mob: 9433814081; fax: +91 343 2546 745. E-mail addresses: pr_banerjee@cmeri.res.in, priyabratabanerjee16@gmail.com Webpage: www.cmeri.res.in and www.priyabratabanerjee.in*

[b.] *Academy of Scientific and Innovative Research (AcSIR), AcSIR Headquarters CSIR-HRDC Campus, Postal Staff College Area, Sector 19, Kamla Nehru Nagar, Ghaziabad-201002, Uttar Pradesh, India.*

[c.] *Department of Microbiology, The University of Burdwan, Golapbag, Bardhaman-713104, West Bengal, India.*

Fig. S1 ESI-MS data of **DNMH** [Inset Yellow coloured **DNMH**]

Fig. S2 ^{1}H-NMR Spectra of **DNMH** in ACN-d$_3$

Fig. S3 Extended **i**ntra and intermolecular H-bonding network in **DNMH**.
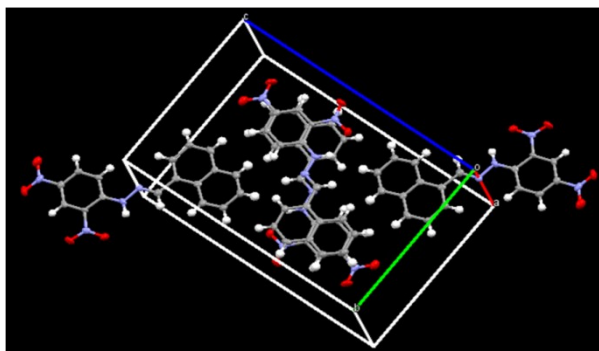
Fig. S4 SCXRD packing arrangement of **DNMH** in unit cell having four molecules.

Table S1. Crystal data of **DNMH**

Crystal Data	
Formula	$C_{17} H_{12} N_4 O_4$
Formula Weight	336.31
Crystal System	monoclinic
Space group	P21/n (No. 14)
a, b, c [Angstrom]	6.787(2) 12.178(5) 17.714(7)
alpha, beta, gamma [deg]	90 98.997(11) 90
Volume	1446.1(9) Å^3
Z	4
D(calc) [g/cm^3]	1.545
Mu(MoKa) [/mm]	0.114
F(000)	696
Crystal Size [mm]	0.12 x 0.14 x 0.18
Data Collection	
Temperature (K)	120
Radiation [Angstrom]	MoKa 0.71073
Theta Min-Max [Deg]	2.3, 25.0
Dataset	-8: 7 ; -14: 14 ; -21: 21
Tot., Uniq. Data, R(int)	10216, 2539, 0.105
Observed Data [I > 2.0 sigma(I)]	1613
Refinement	
Nref, Npar	2539, 226
R, wR2, S	0.0945, 0.2092, 1.14
w =	^2^(FO^2^)+(0.0364P)^2^+4.8771P] WHERE P=(FO^2^+2FC^2^)/3'
Max. and Av. Shift/Error	0.00, 0.00
Min. and Max. Resd. Dens. [e/Ang^3]	-0.34, 0.35

Table S2. Bond Distances (Angstrom) of **DNMH**

Bond Distances (Angstrom)					
O1	-N2	1.222(6)	C00F	-C00H	1.479(8)
O001	-N1	1.241(5)	C00G	-C00I	1.360(7)
O002	-N1	1.225(6)	C00J	-C00O	1.419(8)
O004	-N2	1.240(7)	C00J	-C00L	1.358(7)
N1	-C009	1.455(7)	C00K	-C00N	1.425(7)
N005	-N007	1.379(6)	C00K	-C00P	1.426(7)
N005	-C00A	1.352(6)	C00M	-C00N	1.392(7)
N2	-C00D	1.443(6)	C00O	-C00P	1.353(8)
N007	-C00H	1.273(6)	C00B	-H00B	0.9500
C009	-C00A	1.430(7)	C00C	-H00C	0.9500
C009	-C00B	1.376(7)	C00G	-H00G	0.9500
N005	-H005	0.8800	C00H	-H00H	0.9500
C00A	-C00I	1.410(7)	C00I	-H00I	0.9500
C00B	-C00D	1.378(8)	C00J	-H00J	0.9500
C00C	-C00M	1.402(7)	C00L	-H00L	0.9500
C00C	-C00F	1.364(7)	C00M	-H00M	0.9500
C00D	-C00G	1.387(8)	C00N	-H00N	0.9500
C00E	-C00F	1.422(7)	C00O	-H00O	0.9500
C00E	-C00L	1.443(8)	C00P	-H00P	0.9500
C00E	-C00K	1.420(7)			

Table S3. Bond Angles (Degrees) of **DNMH**

O001	-N1	-O002	123.2(4)	N007	-C00H	-C00F	119.1(5)
O001	-N1	-C009	118.8(4)	C00A	-C00I	-C00G	122.7(5)
O002	-N1	-C009	118.1(4)	C00L	-C00J	-C00O	120.4(5)
N007	-N005	-C00A	117.8(4)	C00E	-C00K	-C00N	119.5(5)
O1	-N2	-O004	122.9(4)	C00N	-C00K	-C00P	120.2(5)
O1	-N2	-C00D	117.8(5)	C00E	-C00K	-C00P	120.3(5)
O004	-N2	-C00D	119.3(4)	C00E	-C00L	-C00J	121.8(5)
N005	-N007	-C00H	115.7(4)	C00C	-C00M	-C00N	118.8(5)
N1	-C009	-C00A	121.9(5)	C00K	-C00N	-C00M	120.1(4)
N1	-C009	-C00B	116.7(4)	C00J	-C00O	-C00P	120.2(5)

C00A	-C009	-C00B	121.4(5)	C00K	-C00P -C00O	120.8(5)
N007	-N005	-H005	121.00	C009	-C00B -H00B	120.00
C00A	-N005	-H005	121.00	C00D	-C00B -H00B	120.00
N005	-C00A	-C009	124.0(5)	C00F	-C00C -H00C	118.00
N005	-C00A	-C00I	120.4(4)	C00M	-C00C -H00C	118.00
C009	-C00A	-C00I	115.5(5)	C00D	-C00G -H00G	120.00
C009	-C00B	-C00D	120.3(5)	C00I	-C00G -H00G	120.00
C00F	-C00C	-C00M	123.1(5)	N007	-C00H -H00H	120.00
N2	-C00D	-C00G	120.3(5)	C00F	-C00H -H00H	120.00
C00B	-C00D	-C00G	120.0(5)	C00A	-C00I -H00I	119.00
N2	-C00D	-C00B	119.7(5)	C00G	-C00I -H00I	119.00
C00K	-C00E	-C00L	116.6(5)	C00L	-C00J -H00J	120.00
C00F	-C00E	-C00K	119.4(5)	C00O	-C00J -H00J	120.00
C00F	-C00E	-C00L	123.9(5)	C00E	-C00L -H00L	119.00
C00E	-C00F	-C00H	120.8(5)	C00J	-C00L -H00L	119.00
C00C	-C00F	-C00H	120.2(5)	C00C	-C00M -H00M	121.00
C00C	-C00F	-C00E	119.0(5)	C00N	-C00M -H00M	121.00
C00D	-C00G	-C00I	120.1(5)	C00K	-C00N -H00N	120.00

Table S4. Bond Angles (Degrees) (continued) of **DNMH**

C00M -C00N -H00N	120.00	C00K -C00P -H00P	120.00
C00J -C00O -H00O	120.00	C00O -C00P -H00P	120.00
C00P -C00O -H00O	120.00		

Table S5. Hydrogen bonding in **DNMH** (Angstrom, Deg)

N005 -- H005 .. O001	0.8800	2.0200	2.636(5)	126.00	.
C00B -- H00B .. O002	0.9500	2.3300	2.656(6)	100.00	.
C00C -- H00C .. N007	0.9500	2.4500	2.785(7)	100.00	.
C00H -- H00H .. O004	0.9500	2.4700	3.223(7)	136.00	4_454
C00I -- H00I .. N007	0.9500	2.3600	2.709(6)	101.00	.
C00I -- H00I .. O004	0.9500	2.5800	3.314(7)	134.00	2_556

Solvatochromic behaviour of DNMH

Solvatochromism is generally induced by changing the environment of the solvent in which the solute undergoes dissolution owing to non-specific interactions including polarity, dielectric constant, dipole moment, polarity, π-conjugation, acid-base chemistry, charge transfer and specific interactions like hydrogen bonding.[1] In this case it is vital to interpret how actually hydrogen bonding, polarity and polarizability of the solvent affect the absorption maxima. Therefore, the electronic spectra of **DNMH** have been recorded in a series of solvents of varying polarity: Acetonitrile, Dichloromethane, Hexane, Methanol, Tetrahydrofuran, Dimethylsulfoxide, Toluene, Xylene, Benzene, Chloroform, Dioxane, Ethanol, Isopropanol and Water (Fig. S5). **DNMH** displayed absorption maxima around 390 nm for ACN,

DCM, CHCl$_3$, MeOH and THF whereas bathochromic shift for polar solvents *like* DMSO by ~20nm and hypsochromic shift for non-polar solvents *like* Hexane by ~10 nm was observed. Hexane, having the least polarity (0.009), *i.e.*, a non-polar solvent exhibited a blue shift in the absorption spectra. On the contrary although DMSO has comparable polarity with acetonitrile (DMSO: 0.444 and ACN: 0.46) and much lesser than MeOH (0.762), EtOH (0.654), 2-propanol (0.546) yet due to its appreciably high dielectric constant (46.7) in comparison to the highly polar solvents; MeOH (32.7), EtOH (24.55), Isopropanol (19.92) and high hydrogen bond acceptance value altogether causes **DNMH** to exhibit positive solvatochromism in presence of DMSO solvent. In general, the shifting in polar solvents may be attributed to the alteration in charge density of the solute (DNMH) occurring on optical excitation; whereas in nonpolar solvents devoid of permanent dipole moment, their electron clouds are polarized by the charge density of the solute (DNMH) along with a feeble degree of inductive interaction and dispersive solute-solvent interaction, which results in the spectral shift.[2]
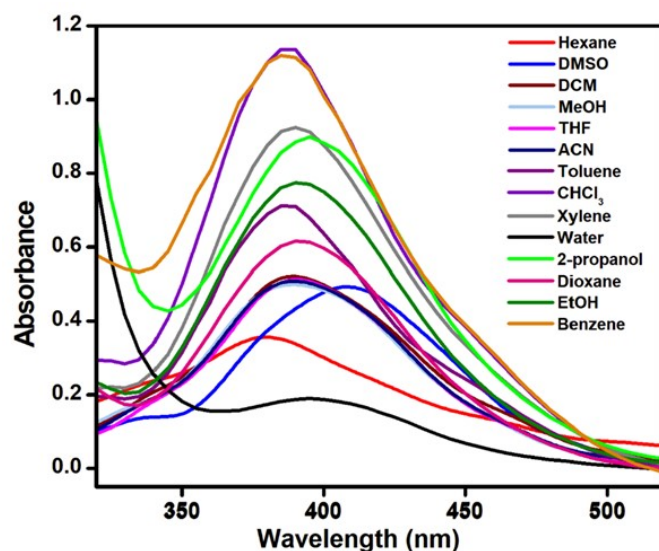
Fig. S5 Spectrophotometric response of **DNMH** in varying solvents Acetonitrile, Dichloromethane, Hexane, Methanol, Tetrahydrofuran, Dimethylsulfoxide, Toluene, Xylene, Benzene, Chloroform, Dioxane, Ethanol, Isopropanol and Water.

Colorimetric response and optical performance of the chemoreceptor **DNMH** with CN⁻ has been investigated in organo-aqueous mixture of varying stoichiometry. This has been purposefully performed to validate the best solvent mixture ratio wherein chromogenic detection of CN⁻ is the most promising.

In this consequence, the colorimetric response of **DNMH** has been studied in presence of CN⁻ in various solvent mixtures; H$_2$O, MeCN: H$_2$O (1:1 v/v), MeCN: H$_2$O (2:1 v/v), MeCN: H$_2$O (3:1 v/v), MeCN: H$_2$O (4:1 v/v) keeping the total volume of (sensor + analyte) constant (Fig. S6†). The outcome of "naked eye" response clearly demonstrated that the chromogenic change of **DNMH** in existence of CN⁻ even in purely aqueous medium was unambiguously obvious. Nevertheless, in MeCN: H$_2$O (4:1, v/v), the detection of CN⁻ is the most promising which is noticeable from the appearance of red coloration due to strong adduct formation. The UV-Vis spectral response further supported the choice of MeCN: H$_2$O=4:1 (v/v) to be the optimal solvent concentration owing to the maximum change in absorbance of **DNMH** with CN⁻ in this solvent mixture (Fig. S7†).
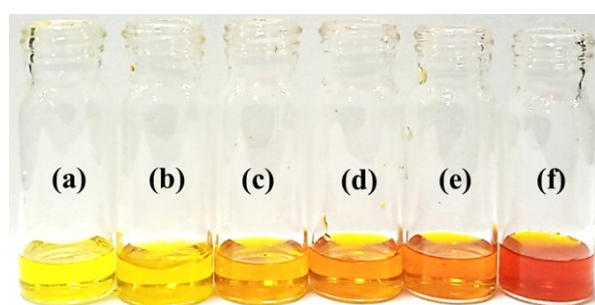
Fig. S6 Colorimetric changes of **DNMH** with CN⁻ in varying proportion of CH$_3$CN and H$_2$O; **(a)** DNMH (1×10⁻⁵M, ACN), **(b)** DNMH + CN⁻ (Water), **(c)** DNMH + CN⁻ (MeCN: Water= 1:1(v/v)), **(d)** DNMH + CN⁻ (MeCN : Water= 2:1(v/v)), **(e)** DNMH + CN⁻ (MeCN : Water= 3:1(v/v)), **(f)** DNMH + CN⁻ (MeCN : Water= 4:1(v/v).
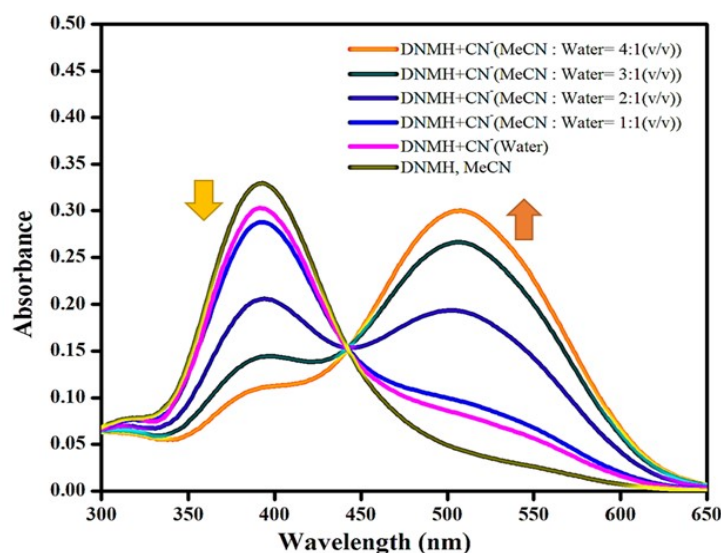
Fig. S7 UV-Vis absorption changes of **DNMH** with gradual addition of CN⁻ in varying solvent mixture; H_2O, MeCN: H_2O (1:1 v/v), MeCN: H_2O (2:1 v/v), MeCN: H_2O (3:1 v/v), MeCN: H_2O (4:1 v/v).
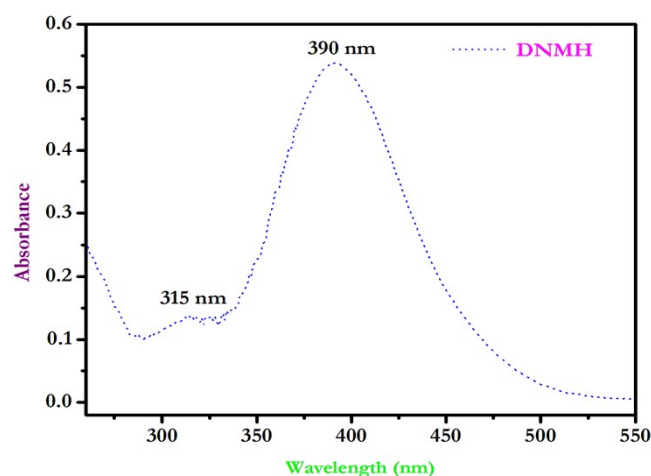
Fig. S8 UV-Vis spectra of **DNMH** (2×10^{-5}M) in acetonitrile.

Jobs Plot of DNMH with CN⁻

The stoichiometric ratio of the chemosensor **DNMH** with CN⁻ successive solutions comprising of 10^{-4} M NBu₄CN and **DNMH** were prepared in acetonitrile solvent in such a way that the total concentration of the resulting solution remains constant. The mole fraction of the added analyte CN⁻ was varied from 0.1 to 0.9. The absorbance of the chemosensor **DNMH** at 510 nm has been plotted against the mole fraction of the added analyte. From the Jobs Plot analysis, it clearly affirms a 1:1 type host: guest complexation.
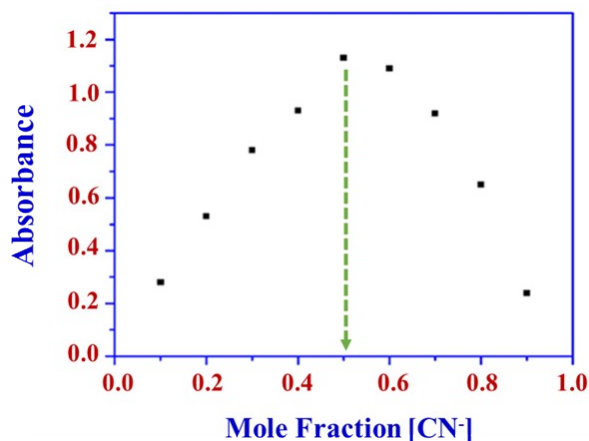
Fig. S9 Jobs plot of **DNMH** with CN.

Benesi-Hildebrand (B-H) Equation and Plot:

The association constant of adduct formed during interaction between the chemosensor (host) and incoming targeted analyte (guest) can be determined by the following complex equilibrium.

$$L + mX^{n-} \rightleftharpoons (X_mL)^{mn-}$$
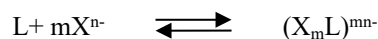
Hence the association constant can be determined as,

$$K_a = \frac{[(X_mL)]^{mn-}}{[L][X^{n-}]^m}$$

Where $[X^{n-}]$, $[L]$ and $[(X_mL)]^{mn-}$ are the concentration of the guest analyte, chemosensor and host-guest adduct respectively.

For 1:1 stoichiometry (m=1), Linear Benesi-Hildebrand equation can be expressed in terms of optical density (A) as follows

$$A = \frac{A_0 + A_1K[X^{n-}]}{1 + K[X^{n-}]}$$

$$\frac{1}{A - A_0} = \frac{1}{K_a(A_{max} - A_0)[guest]^1} - \frac{1}{A_{max} - A_0}$$

Where A_0 and A indicate the optical density or absorbance at a particular wavelength of **DNMH** in the absence of the guest analyte (CN^-) and presence of guest analyte in each successive step respectively and A_{max} represents the maximum absorbance, *i.e*; the saturated absorbance of the chemosensor molecule in presence of excess analyte; [guest] is the concentration of guest ion added and K_a is the complex association constant. Where $[X^{n-}]$, $[L]$ and $[(X_mL)^{mn-}]$ are the concentration of the added targeted analyte, chemosensor and the complexation between the analyte and the chemosensor respectively. A_o, A and A_1 prior to the addition of the analyte, absorbance after adding the analyte at every successive step and finally excess amount of the added analyte, respectively. The binding constant or association constant K (M^{-1}) is determined from the ratio of slope and intercept of Benesi-Hildebrand plot of optical density. As depicted in the following In the Benesi-Hildebrand (B-H) plot of $1/[A-A_0]$ *vs* $1/[CN^{-1}]$ for the titration of the chemosensor **DNMH** and CN^-, provides a straight line (best fitted), indicating a 1:1 type complex formation. The association constant K_a for CN^- is 4.48 $\times 10^6$ M^{-1}
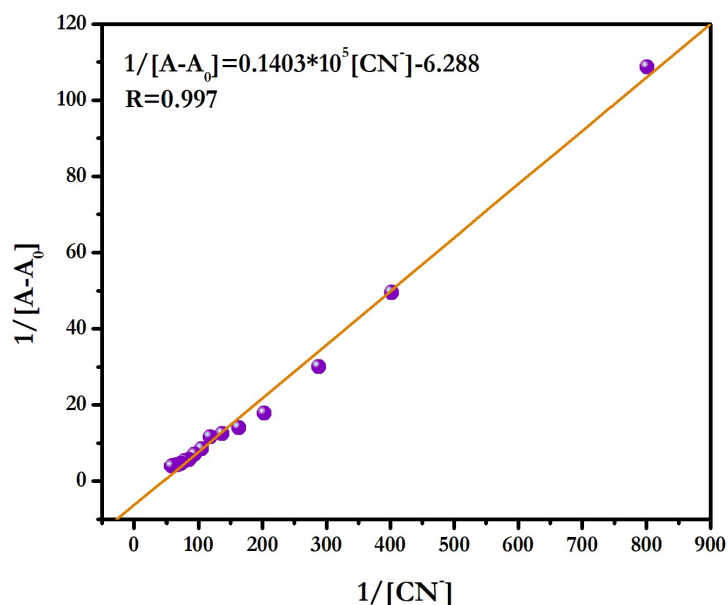
Fig. S10 Benesi-Hildebrand plot for absorbance of CN^- with **DNMH** for the association constant determination.

Limit of detection

The detection limit (DL) has been calculated following UV-Vis titration. The absorbance spectrum of **DNMH** was repeated for 10 times, and its standard deviation is measured. The limit of detection (LOD) is calculated from the following formula: DL = 3σ/k. σ is the standard deviation of the blank solution of **DNMH**. Gradual emergence of new absorbance values during colorimetric titration with targeted analytes is plotted against its concentration. The (k) is derived from the slope of these plots.

$A-A_0 = 19.095 \times 10^{-5} M \ [CN^-] - 0.0178$

$R^2 = 0.998$
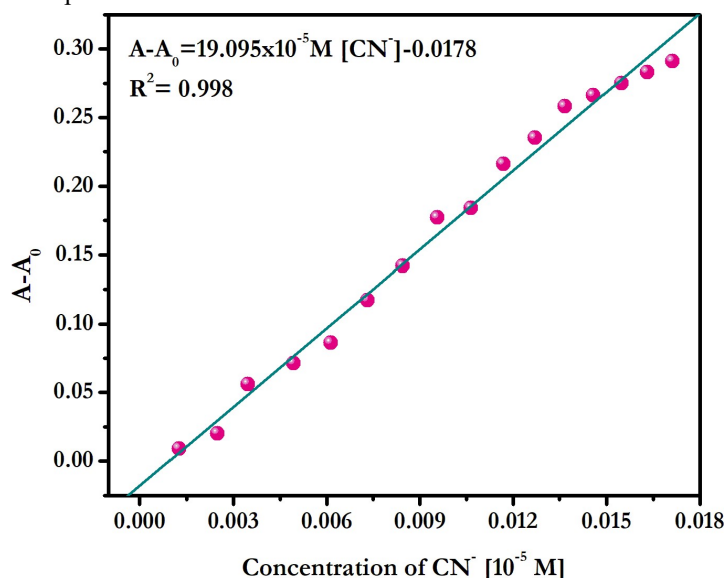
Fig. S11 Change of absorbance at 510 nm as the linear function of the concentration of CN^- for the calculation of LOD of **DNMH** towards CN^-.

$R^2 = 0.996$

k = 6.314 g/mg.sec
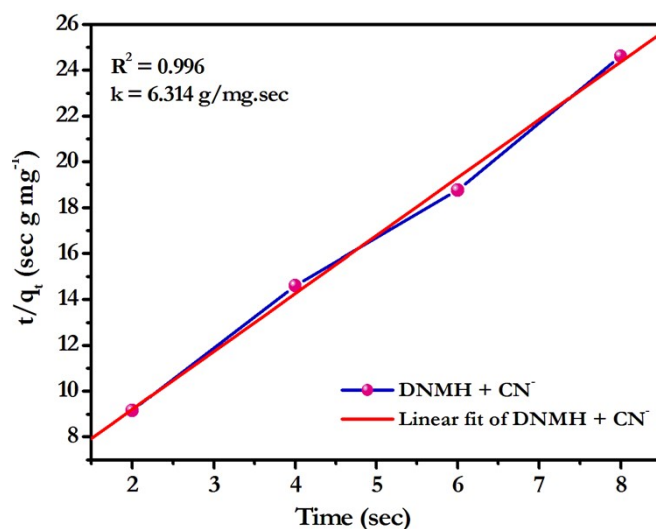
Fig. S12 Pseudo second order reaction kinetics of **DNMH** with CN^-.

Time evolution and Kinetic study of DNMH in existence of CN^-. In order to determine the practical applicability of **DNMH** towards target specific analyte detection, photo stability of the chemosensor in presence of guest analyte (CN^- herein) is significant. The time dependant host: guest interaction has been recorded by taking the UV-Vis spectroscopic data upon addition of 5 equivalents of CN^- in ACN: H_2O (4:1, *v/v*) into **DNMH** (2×10^{-5}M, ACN) solution. A very feeble change in the absorption spectra was observed with increasing time which implicates high photostability of the resultant adduct. From the kinetics profile it was observed that the faster reaction rate of **DNMH** towards CN^- displays a pivotal role underlying the practical applicability of the chemosensor.
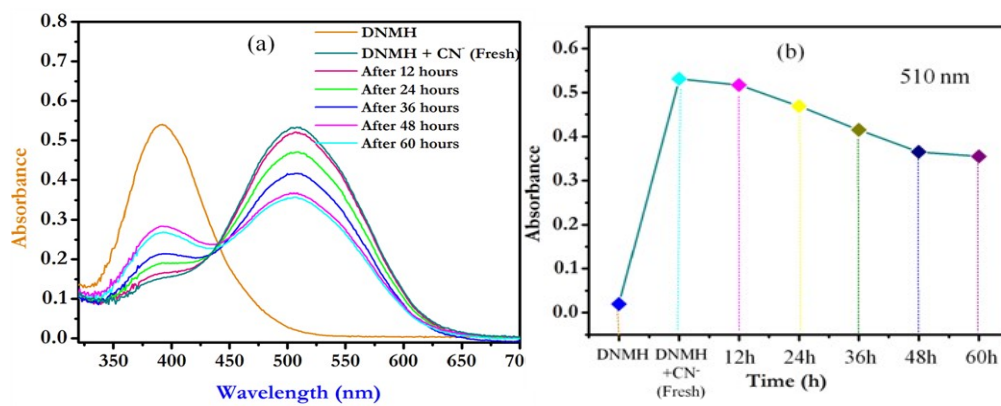
Fig. S13
Time

dependant spectral response of **DNMH** (2×10^{-5}M, ACN) in existence of 5 equivalent of CN⁻ (ACN: water, 4:1 v/v) **(a)** plot of Absorbance *vs* wavelength; **(b)** plot of absorbance vs time (h).

Electrochemical properties of **DNMH** with CN⁻ have been investigated by using cyclic voltammetry. During this study TBAPF$_6$ as supporting electrolyte, glassy carbon as working electrode, Ag/AgCl electrode as reference electrode and platinum wire as the counter electrode has been used.
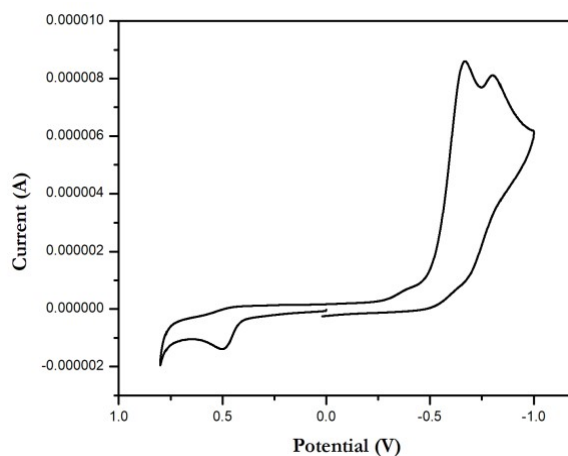
Fig. S14 Cyclic voltammogram of **DNMH** in acetonitrile.
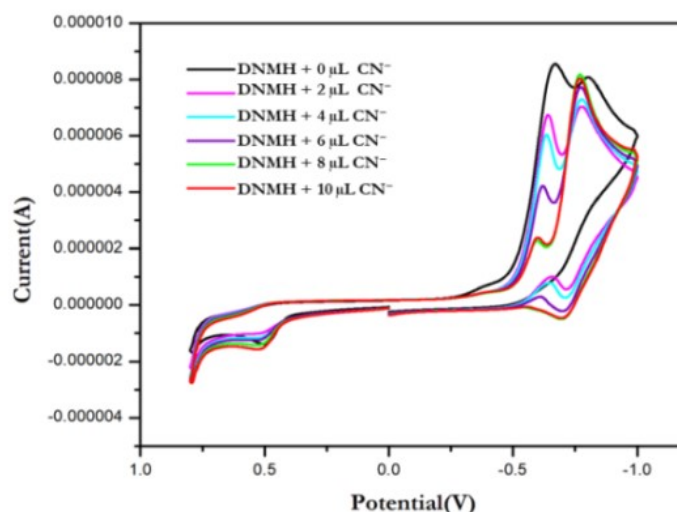
Fig. S15 Electrochemical response of **DNMH** in ACN with CN⁻ (10^{-3}M, ACN) in existence of TBAPF$_6$ as supporting electrolyte; scan rate 0.05 Vs⁻¹.

Table S6. Redox potential of **DNMH** with CN⁻

Host•••Guest	DNMH•••CN⁻
Initial Oxidation	**Ep = 0.50 V** **Ip = -0.00138 mA**
Initial Reduction	**Ep = -0.66 V** **Ip = 0.0086 mA**
Final Oxidation	**No Oxidation**
Final Reduction	**Ep = -0.59 V** **Ip = 0.0023 mA**
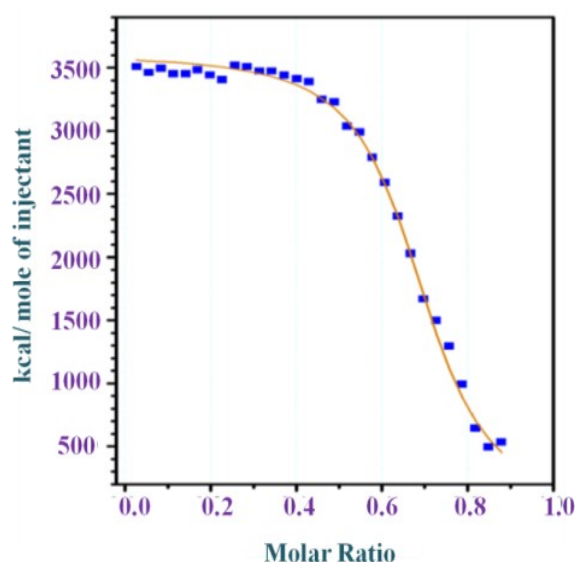
Fig. S16 Isothermal calorimetric titration of **DNMH** with CN⁻ in ACN at 298 K.

The [**DNMH•••CN⁻**] ensemble was utilized to investigate its reversibility in presence of any cation. In this context, the sensing experiment was performed by adding 200µL solutions of different cations (10^{-4}M) to 500µL solution of the [**DNMH•••CN⁻**] adduct. It was observed that the reddish orange color of the ensemble changed to light yellow in the presence of only Cd^{2+}, whereas for the other cations, the color of the adduct solution remained unperturbed (Fig. S17†). This indicates the profound selective nature of the ensemble towards Cd^{2+} only and therefore, this divalent ion was chosen to establish the reversibility process of **DNMH**+CN⁻ ensemble.
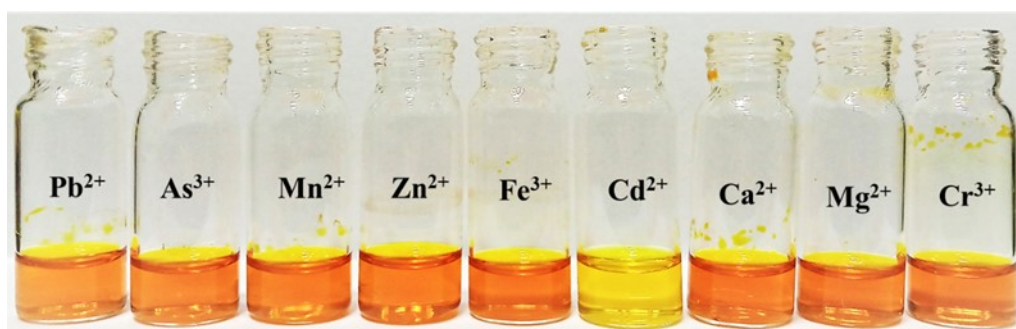
Fig. S17 Colorimetric response of **DNMH•••CN⁻** ensemble in presence of varying cations.

Proposition of electronic circuit based on different logic gate:
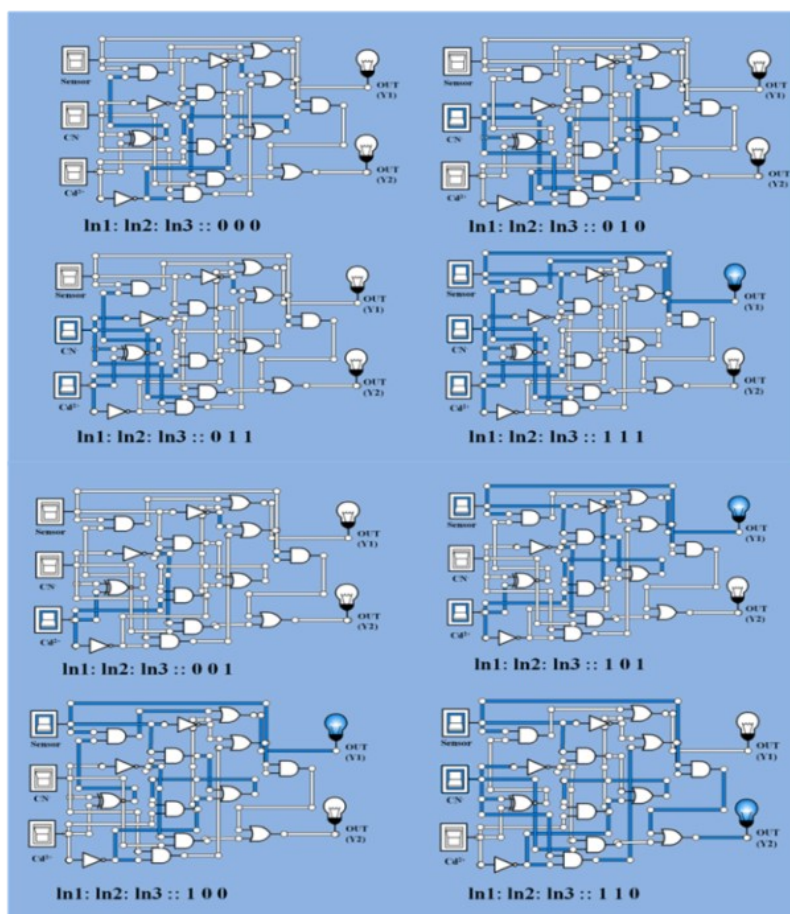
Fig. S18 Proposition of logic gate by changing the inputs AND-NOT-XNOR-NAND-OR logic functions.

Table S7. Truth table for molecular logic operation.

In1 (S2)	In2 (CN⁻)	In3 (Cd²⁺)	OUT Y1 (390 nm)	OUT Y2 (510 nm)
0	0	0	0 (Low)	0 (Low)
0	1	0	0 (Low)	0 (Low)
0	0	1	0 (Low)	0 (Low)
1	0	0	1 (High)	0 (Low)
1	0	1	1 (High)	0 (Low)
1	1	0	0 (Low)	1(High)
0	1	1	0 (Low)	0 (Low)

Dynamic Light Scattering (DLS) Analysis

DNMH in ACN medium acquires a partial aggregated form due to weak intermolecular hydrogen bonding between the 2° amine centre and imine centre of **DNMH** with the solvent molecules which causes the average particle size to be 75 nm as observed from DLS analysis. However, after CN$^-$ addition, the self-aggregation of **DNMH** molecule is disrupted by minimizing the solvation effect. Consequently, the population density of **DNMH** in presence of CN$^-$ exhibited two peaks with reduced size distribution <10 nm (Fig. S16†) due to non-covalent weak hydrogen bonding interactions between the antenna centres (-NH-, -CH=N-) of **DNMH** with the incoming CN$^-$.[3]
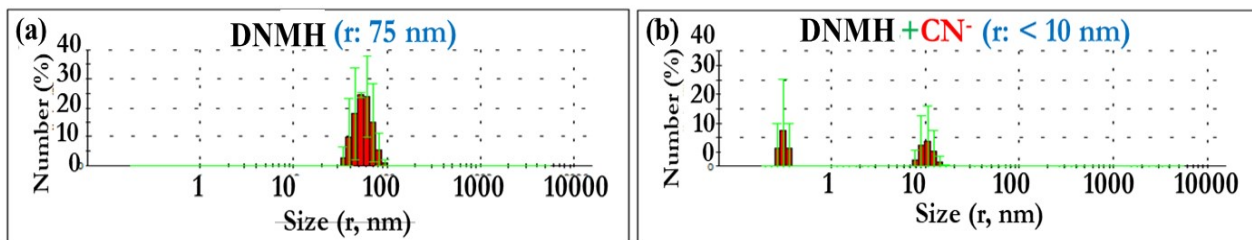
Fig. S19 DLS analysis of a) **DNMH** (1×10^{-4}M, CH$_3$CN), b) **DNMH** + CN$^-$ in CH$_3$CN: H$_2$O (4:1).

FT-IR study

The FT-IR spectroscopy of **DNMH** has been carried out by using the KBr disks. The 3400 cm^{-1} and 1618 cm^{-1} peak suggests the presence of secondary amine and aldimine bond in **DNMH**. Upon addition of CN$^-$ the electron density on the -NH bond drifted towards -N atom of –CN owing to the intermolecular H-bonding interaction (-NH•••NC$^-$) and furthermore the lone pairs on the N-atom undergo delocalisation. Therefore, the NH bond becomes weak and broadened in nature. Additionally, the peak at 1618 cm^{-1} also swinged to the lower frequency region (1600 cm^{-1}) due to H-bonding (–N=CH•••NC$^-$). The peaks within the range 1600 cm^{-1} to 500 cm^{-1} also become flattened due to enhancement of electronic distribution all over the molecular scaffold (Fig. S17†).
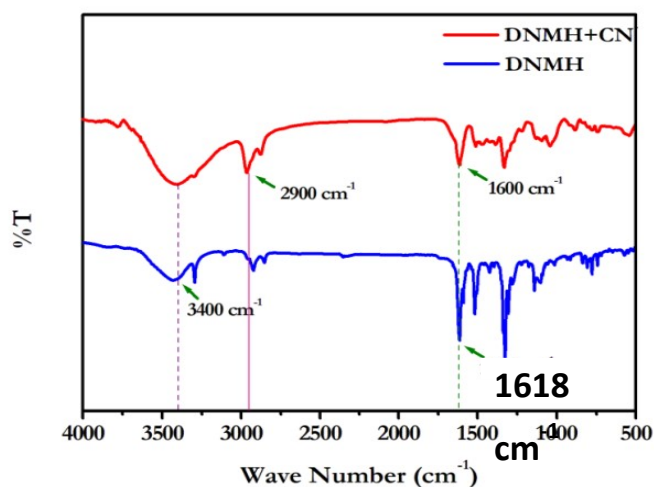
Fig. S20 FT-IR Spectroscopy of **DNMH** and **DNMH**•••CN$^-$ complex.

Antibacterial Assay

A quantification of cellular growth and inhibition can be well understood from the cytotoxicity study. For the purpose of preliminarily counting and culturing of the cells, 24-well plates and centrifuge tubes have been utilized. At the initial stage the cells have been incubated at ambient conditions and thereby observed at regular time interval. The in vitro cytotoxicity assay study has been performed in the microtiter well plates during their logarithmic phase after 12-16 h of incubation. The Bt and E. *Coli* cells are then centrifuged to form pellets and subsequently washed with saline water. A wide range of varying concentration of the cytotoxic agent (**DNMH**), 10^{-2}M-10^{-7}M has been added to the previously formed cell pellets in separate tubes. The cells are then suspended *via* mild vortexing followed by incubation at 37˚C for 2 hrs. The treated cells are centrifuged again and the pellets are washed with normal saline and suspended in sterile broth medium followed by its incubation for 2-4 hrs at 37˚C. After incubation the MTT reagent (3-(4,5-dimethylthiazol-2-yl)-2,5-diphenyl tetrazolium bromide) is added in individual tubes which is further subjected to 2-4 hrs incubation at 37˚C until formation of purple coloured formazan crystals. A comparative study has been performed taking into consideration

one positive control (contains no cytotoxic agent), one negative control (contains only the broth and the MTT reagent) and one blank (contains only the broth). For terminating the reaction as well as dissolving the so formed formazan crystals acidic isopropanol is added following the process of incubation. After addition of the solubilising agent all the contents were thoroughly mixed and further subjected to 1hr incubation at 37˚C for complete dissolution of the obtained formazan crystals. The spectrophotometric reading is taken at 570 nm wherein the absorbance measurement of the formazan is taken separately. The entire spectrophotometric study has been performed for individual set that has been taken in triplicate.

Time Dependant Density Functional Theoretical (TDDFT) calculation. To congregate detailed information regarding the experimentally obtained absorption bands of **DNMH** and DNMH•••CN⁻, TDDFT calculations have been performed. B3LYP hybrid functional and defSV(P)/defTZVP were used in Turbomole (V7.0) software TmoleX interface, 4.1.1. The experimental along with simulated spectra (applying COSMO/acetonitrile) of **DNMH**, **DNMH•••CN⁻** are shown in Fig. S18†. In case of **DNMH**, the simulated peak at 390 nm is in good agreement with the experimentally obtained λ_{max} at 425 nm. For **DNMH•••CN⁻** adduct, the theoretical peak at 510 nm appeared close to its experimentally resolved λ_{max} at 550 nm. The major electronic excitation calculations and the coordinates for TDDFT of **DNMH** and **DNMH•••CN⁻** have been presented in Table S8-S10†.
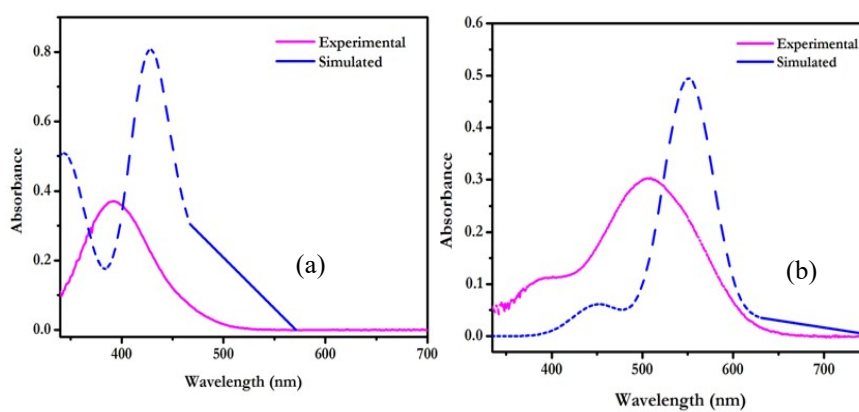
Fig. S21 Experimental and simulated UV-Vis spectrum of (a) **DNMH** and (b) **DNMH** + CN⁻ (Simulation

done at TDDFT/B3LYP/defSV(P)/dEFTZVP level of theory).

Table S8. Major electronic excitation calculated by TDDFT in Turbomole (V7.0) software TMoleX interface, 4.1.1.

Chemosensor	λ_{max} (Experimental)	λ_{max} (Theoretical)	Energy (eV)	Oscillator Strength
DNMH	390	425	2.97	0.7887
DNMH + CN⁻	510	550	1.72	0.4921
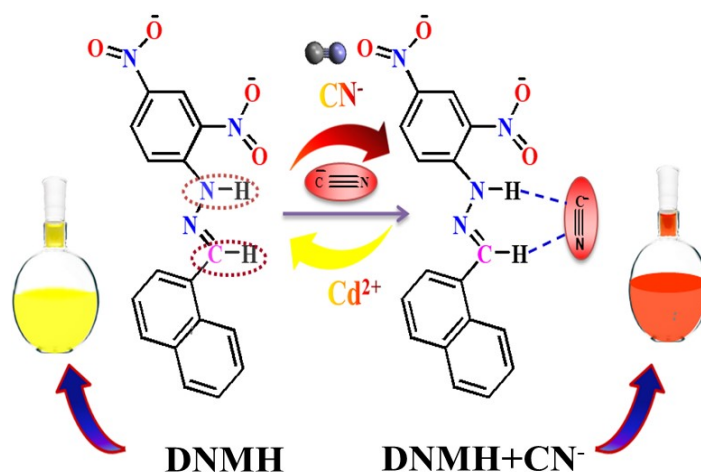
Fig. S22 The plausible mechanistic course of interaction of **DNMH** with CN⁻.

Table S9. Coordinates for TDDFT of **DNMH**

Frequency	Oscillator strength
234.76840115	0.00000063
237.13851714	0.00000115
239.50863313	0.00000207
241.87874912	0.00000366
244.24886511	0.0000064
246.6189811	0.00001103
248.98909708	0.00001877
251.35921307	0.00003149
253.72932906	0.00005214
256.09944505	0.00008515
258.46956104	0.0001372
260.83967703	0.00021806
263.20979302	0.00034188
265.579909	0.00052876
267.95002499	0.00080673
270.32014098	0.00121414
272.69025697	0.00180255
275.06037296	0.00263989
277.43048895	0.00381383
279.80060493	0.00543523
282.17072092	0.00764117
284.54083691	0.01059719
286.9109529	0.01449827
289.28106889	0.01956787
291.65118488	0.02605443
294.02130087	0.03422472
296.39141685	0.04435378

298.76153284	0.05671102
301.13164883	0.07154278
303.50176482	0.08905199
305.87188081	0.10937571
308.2419968	0.13256233
310.61211278	0.15855007
312.98222877	0.18714908
315.35234476	0.21802922
317.72246075	0.25071553
320.09257674	0.28459303
322.46269273	0.31892159
324.83280872	0.35286101
327.2029247	0.38550521
329.57304069	0.41592364
331.94315668	0.44320729
334.31327267	0.46651575
336.68338866	0.48512206
339.05350465	0.49845165
341.42362063	0.50611275
343.79373662	0.50791597
346.16385261	0.50388204
348.5339686	0.49423782
350.90408459	0.47940144
353.27420058	0.45995877
355.64431657	0.43663357
358.01443255	0.41025425
360.38454854	0.38172011
362.75466453	0.35196947
365.12478052	0.32195163
367.49489651	0.29260395
369.8650125	0.26483442
372.23512848	0.23950927
374.60524447	0.21744469
376.97536046	0.19940093
379.34547645	0.18607686
381.71559244	0.17810289
384.08570843	0.17603044
386.45582442	0.18031647
388.8259404	0.19130247
391.19605639	0.20918807
393.56617238	0.23400082
395.93628837	0.26556448
398.30640436	0.30346955
400.67652035	0.34705017
403.04663633	0.39537199
405.41675232	0.44723543
407.78686831	0.50119768
410.1569843	0.55561536
412.52710029	0.60870791
414.89721628	0.65863914
417.26733227	0.70361242
419.63744825	0.74197256
422.00756424	0.77230616
424.37768023	0.79353153
426.74779622	0.80496947
429.11791221	0.80638787

431.4880282	0.79801493
433.85814418	0.78051927
436.22826017	0.75495789
438.59837616	0.72269664
440.96849215	0.68531015
443.33860814	0.64447046
445.70872413	0.60183408
448.07884012	0.55893755
450.4489561	0.51710977
452.81907209	0.47740772
455.18918808	0.44057937
457.55930407	0.40705475
459.92942006	0.37696327
462.29953605	0.35017325
464.66965203	0.32634772
467.03976802	0.30500961
571.32487152	0.00000086

Table S10. Coordinates for TDDFT of **DNMH•••CN**-

Frequency	Oscillator strength
321.35222227	0.00000072
324.51339905	0.00000125
327.67457583	0.00000213
330.8357526	0.00000358
333.99692938	0.00000594
337.15810616	0.00000971
340.31928294	0.00001568
343.48045971	0.00002498
346.64163649	0.00003925
349.80281327	0.00006085
352.96399005	0.00009307
356.12516682	0.00014044
359.2863436	0.00020909
362.44752038	0.00030711
365.60869715	0.00044505
368.76987393	0.00063628
371.93105071	0.00089749
375.09222749	0.00124897
378.25340426	0.00171479
381.41458104	0.00232278
384.57575782	0.00310415
387.7369346	0.00409276
390.89811137	0.00532389
394.05928815	0.0068325
397.22046493	0.00865105
400.3816417	0.0108068
403.54281848	0.01331878
406.70399526	0.01619464
409.86517204	0.01942758
413.02634881	0.02299362
416.18752559	0.02684967
419.34870237	0.03093259
422.50987915	0.03515952
425.67105592	0.03942983

428.8322327	0.04362859
431.99340948	0.04763166
435.15458625	0.05131207
438.31576303	0.05454753
441.47693981	0.05722842
444.63811659	0.05926591
447.79929336	0.06059957
450.96047014	0.06120405
454.12164692	0.06109433
457.2828237	0.0603294
460.44400047	0.05901418
463.60517725	0.05729966
466.76635403	0.05538155
469.9275308	0.0534975
473.08870758	0.05192313
476.24988436	0.05096698
479.41106114	0.05096439
482.57223791	0.05227008
485.73341469	0.05524921
488.89459147	0.06026638
492.05576825	0.06767233
495.21694502	0.07778789
498.3781218	0.09088528
501.53929858	0.10716702
504.70047535	0.12674345
507.86165213	0.14961003
511.02282891	0.17562654
514.18400569	0.20450028
517.34518246	0.23577574
520.50635924	0.26883313
523.66753602	0.30289751
526.8287128	0.33705987
529.98988957	0.3703101
533.15106635	0.40158089
536.31224313	0.42980022
539.4734199	0.45394907
542.63459668	0.47311997
545.79577346	0.48657185
548.95695024	0.49377639
552.11812701	0.49445178
555.27930379	0.48858083
558.44048057	0.47641184
561.60165735	0.45844197
564.76283412	0.43538469
567.9240109	0.40812435
571.08518768	0.37766173
574.24636445	0.34505522
577.40754123	0.31136246
580.56871801	0.27758666
583.72989479	0.24463131
586.89107156	0.21326561
590.05224834	0.18410203
593.21342512	0.15758602
596.3746019	0.13399706
599.53577867	0.11345915
602.69695545	0.09595865

605.85813223	0.08136707
609.019309	0.06946633
612.18048578	0.05997445
615.34166256	0.05257009
618.50283934	0.04691456
621.66401611	0.04267058
624.82519289	0.03951741
627.98636967	0.03716234
631.14754645	0.03534862
760.75579431	0.000001

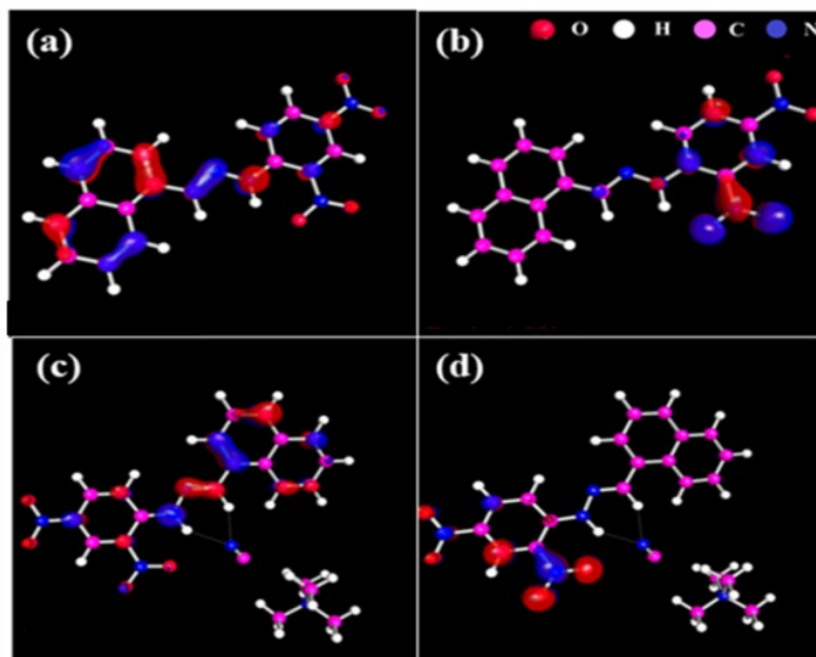**Table S11.** Geometry optimized coordinates of **DNMH**

O	0.5641191	2.2992252	8.3952957
O	0.6128636	0.7667700	9.9087350
O	0.4591261	3.7426301	15.2552273
O	0.5951047	1.7092019	14.5338963
N	0.3938059	4.8465100	9.0518469
N	0.5651332	1.9428624	9.5780545
N	0.3044936	6.1701642	8.8000230
N	0.5148491	2.9186343	14.3491066
C	0.5078360	2.9595683	10.6145321
C	0.4238536	4.3622801	10.3188551
C	0.5368223	2.5007317	11.9344138
C	0.1441757	8.9284558	8.1104692
C	0.4833197	3.4084436	12.9792034
C	0.1176309	8.2808276	5.7464407
C	0.1775574	7.9221244	7.1452498
C	0.3983811	4.7943432	12.7292314
C	0.2713031	6.5195407	7.5588161
C	0.3696208	5.2540089	11.4313617
C	0.0840575	7.7341164	3.3595428
C	0.0233385	9.6760197	5.3986373
C	0.1454045	7.3328603	4.6807729
C	0.0525478	10.2899586	7.7576637
C	-0.0071789	10.6583228	6.4266999
C	-0.0093590	9.1085190	3.0237338
C	-0.0385303	10.0556632	4.0257452
H	0.4366378	4.1648636	8.2873752
H	0.6010713	1.4323050	12.1274015
H	0.1914415	8.6462664	9.1649681
H	0.3566111	5.4935016	13.5652192
H	0.3138653	5.7438182	6.7799233
H	0.3042940	6.3214450	11.2258177
H	0.1078718	6.9819463	2.5649270
H	0.2163152	6.2644849	4.8938122
H	0.0294275	11.0507964	8.5435470
H	-0.0787939	11.7137670	6.1453421
H	-0.0578378	9.4116616	1.9734244
H	-0.1101795	11.1203618	3.7816881

Table S12. Geometry optimized structure of **DNMH•••CN⁻**

O	1.1132480	2.4269030	8.4665878

O	1.1983456	0.8320113	9.9533358
O	0.6267295	3.6803476	15.3780434
O	0.9315731	1.6563751	14.6056856
N	0.5553439	4.9345257	9.1672719
N	1.0599879	2.0221321	9.6424910
N	0.4293000	6.2768868	9.0057819
N	0.7645059	2.8745356	14.4451017
C	0.8399690	3.0042190	10.6976103
C	0.6339123	4.4066764	10.4243023
C	0.8755315	2.5173816	12.0120672
C	0.4089474	9.0855176	8.4565644
C	0.7262485	3.3959897	13.0831473
C	-0.1527359	8.5489064	6.1181548
C	0.1777158	8.1191104	7.4637563
C	0.5442434	4.7832577	12.8598467
C	0.2804117	6.6935933	7.7773268
C	0.5018295	5.2678510	11.5644404
C	-0.7392092	8.1116146	3.7726408
C	-0.2166438	9.9700084	5.8415576
C	-0.4297727	7.6432212	5.0456717
C	0.3360829	10.4688889	8.1759374
C	0.0328257	10.9059062	6.8898359
C	-0.7904715	9.5070787	3.5023453
C	-0.5354762	10.4152776	4.5205974
H	0.5509960	4.2963590	8.3389722
H	1.0309044	1.4449193	12.1808299
H	0.6640240	8.7443254	9.4722573
H	0.4323916	5.4616920	13.7172594
H	0.2200838	5.9448776	6.9616640
H	0.3514573	6.3382788	11.3747184
H	-0.9510689	7.3928719	2.9637781
H	-0.4130171	6.5549304	5.2181303
H	0.5280560	11.1985931	8.9795085
H	-0.0189077	11.9839511	6.6627453
H	-1.0363679	9.8623776	2.4881078
H	-0.5779461	11.5002609	4.3264926
N	-0.2850853	3.9629664	6.2187202
C	-0.9279644	3.3421980	5.4375832
N	-0.3006354	2.0132642	1.9773740
C	0.7396353	3.0412606	2.3462243
C	-1.6693838	2.6434203	2.0601807
C	-0.2309228	0.8677886	2.9567133
C	-0.0486613	1.5114390	0.5820209
H	0.6716479	3.8846455	1.6317659
H	0.5315589	3.3832453	3.3812034
H	1.7397304	2.5700479	2.2830419
H	-0.4400091	1.2765980	3.9674078
H	-0.9919200	0.1151132	2.6727455
H	0.7823131	0.4236149	2.9098194
H	0.9569145	1.0493115	0.5456857
H	-0.8229789	0.7617505	0.3284115
H	-0.1016086	2.3670061	-0.1188661
H	-1.8127023	2.9927167	3.1054569
H	-2.4249741	1.8794813	1.7919569

H	-1.7128013	3.4879434	1.3449783

Fig. S23 Geometry optimized structures (a) HOMO of **DNMH**, (b) LUMO of **DNMH**, (c) HOMO of **DNMH** in presence of CN⁻, (d) LUMO of **DNMH** in presence of CN⁻. [Colour codes: White (H); Magenta (C); Blue (N); Red (O).

Table S13. Geometry optimized coordinates of Fukui Indices for Nucleophilic Attack (Fukui (+)): **DNMH**
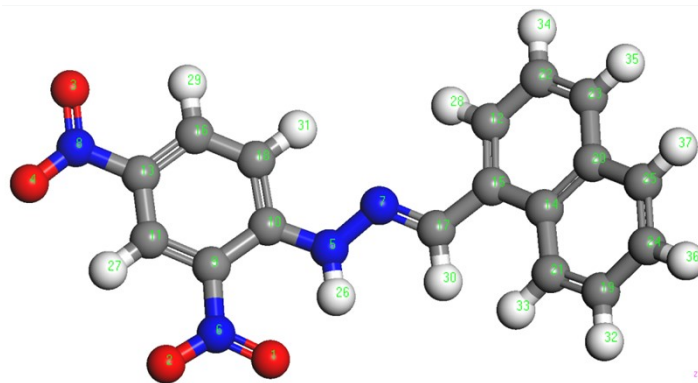
atom	Mulliken	Hirshfeld
O (1)	0.131	0.125
O (2)	0.139	0.131
O (3)	0.081	0.079
O (4)	0.077	0.074
N (5)	0.019	0.025
N (6)	0.080	0.093
N (7)	-0.001	0.008
N (8)	0.043	0.050
C (9)	0.007	0.027
C (10)	0.045	0.034
C (11)	0.087	0.067
C (12)	0.012	0.010
C (13)	0.008	0.028
C (14)	0.006	0.004
C (15)	-0.004	0.003
C (16)	0.043	0.043
C (17)	0.029	0.026

C (18)   0.023   0.031
C (19)   0.004   0.005
C (20)   0.000   0.003
C (21)   0.000   0.002
C (22)   0.001   0.005
C (23)   0.012   0.011
C (24)   0.002   0.003
C (25)   0.003   0.004
H (26)   0.017   0.014
H (27)   0.039   0.030
H (28)   0.006   0.004
H (29)   0.029   0.021
H (30)   0.014   0.009
H (31)   0.026   0.016
H (32)   0.003   0.002
H (33)   0.002   0.002
H (34)   0.005   0.003
H (35)   0.006   0.005
H (36)   0.003   0.002
H (37)   0.003   0.002

Table S14. Geometry optimized coordinates of Fukui Indices for Electrophilic Attack (Fukui (-): **DNMH**

atom	Mulliken	Hirshfeld
O (1)	0.015	0.017
O (2)	0.025	0.025
O (3)	0.019	0.019
O (4)	0.020	0.020
N (5)	0.038	0.043
N (6)	0.008	0.011
N (7)	0.046	0.050
N (8)	0.006	0.009
C (9)	0.024	0.019
C (10)	0.002	0.011
C (11)	0.008	0.011
C (12)	0.047	0.052
C (13)	0.023	0.022
C (14)	0.013	0.017
C (15)	0.050	0.058
C (16)	0.012	0.016
C (17)	0.027	0.030
C (18)	0.024	0.022
C (19)	0.036	0.045
C (20)	0.003	0.018
C (21)	0.049	0.052
C (22)	0.032	0.046
C (23)	0.072	0.075
C (24)	0.031	0.041
C (25)	0.050	0.054
H (26)	0.019	0.015
H (27)	0.012	0.007
H (28)	0.036	0.023

H (29) 0.012   0.008
H (30) 0.029   0.017
H (31) 0.015   0.011
H (32) 0.030   0.021
H (33) 0.031   0.021
H (34) 0.034   0.023
H (35) 0.041   0.029
H (36) 0.029   0.020
H (37) 0.033   0.023

Table S15. Geometry optimized coordinates of Fukui Indices for Nucleophilic Attack (Fukui(+)): **DNMH•••CN⁻**
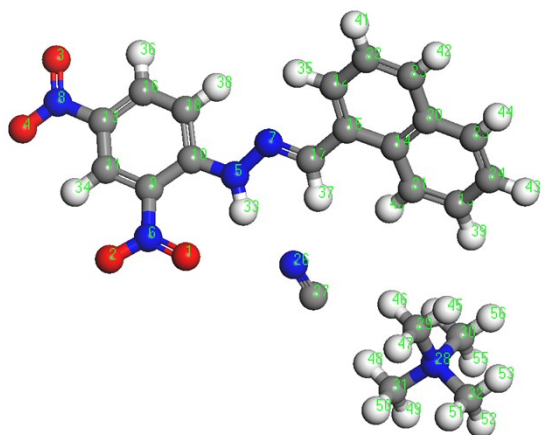
atom	Mulliken	Hirshfeld
O (1)	0.107	0.101
O (2)	0.112	0.106
O (3)	0.108	0.103
O (4)	0.105	0.099
N (5)	0.019	0.023
N (6)	0.063	0.073
N (7)	0.000	0.008
N (8)	0.058	0.068
C (9)	0.008	0.026
C (10)	0.040	0.033
C (11)	0.085	0.068
C (12)	0.013	0.012
C (13)	0.004	0.027
C (14)	0.006	0.004
C (15)	-0.004	0.003
C (16)	0.039	0.038
C (17)	0.031	0.027
C (18)	0.022	0.029
C (19)	0.005	0.005
C (20)	0.000	0.003
C (21)	0.001	0.002
C (22)	0.001	0.005
C (23)	0.014	0.013
C (24)	0.003	0.004
C (25)	0.004	0.004
N (26)	-0.009	-0.001
C (27)	0.013	0.008
N (28)	0.000	0.000
C (29)	0.000	0.000

C (30)	0.000	0.000
C (31)	0.000	0.000
C (32)	0.000	0.000
H (33)	0.009	0.008
H (34)	0.039	0.030
H (35)	0.007	0.005
H (36)	0.030	0.021
H (37)	0.012	0.007
H (38)	0.025	0.016
H (39)	0.004	0.002
H (40)	0.002	0.001
H (41)	0.006	0.003
H (42)	0.007	0.005
H (43)	0.004	0.002
H (44)	0.004	0.003
H (45)	0.001	0.000
H (46)	-0.001	0.000
H (47)	0.000	0.000
H (48)	0.000	0.000
H (49)	0.001	0.000
H (50)	0.000	0.000
H (51)	0.000	0.000
H (52)	0.000	0.000
H (53)	0.000	0.000
H (54)	0.000	0.000
H (55)	0.001	0.000
H (56)	0.000	0.000

Table S16. Geometry optimized coordinates of Fukui Indices for Electrophilic Attack (Fukui (-)): **DNMH•••CN⁻**

Fukui Indices for Electrophilic Attack (Fukui (-))

atom	Mulliken	Hirshfeld
O (1)	0.019	0.019
O (2)	0.030	0.029
O (3)	0.025	0.024
O (4)	0.026	0.025
N (5)	0.047	0.051
N (6)	0.008	0.012
N (7)	0.053	0.055
N (8)	0.006	0.012
C (9)	0.028	0.022
C (10)	0.004	0.013
C (11)	0.009	0.013
C (12)	0.048	0.051
C (13)	0.027	0.027
C (14)	0.012	0.016
C (15)	0.041	0.052
C (16)	0.014	0.019
C (17)	0.035	0.036
C (18)	0.027	0.026
C (19)	0.028	0.036
C (20)	0.002	0.016
C (21)	0.038	0.040
C (22)	0.024	0.039
C (23)	0.068	0.070
C (24)	0.028	0.035

C (25) 0.040   0.044
N (26) -0.004   0.000
C (27) 0.015   0.013
N (28) 0.000   0.000
C (29) -0.001   0.000
C (30) -0.001   0.000
C (31) 0.000   0.001
C (32) 0.000   0.000
H (33) 0.016   0.013
H (34) 0.014   0.008
H (35) 0.035   0.022
H (36) 0.016   0.010
H (37) 0.025   0.014
H (38) 0.018   0.013
H (39) 0.025   0.015
H (40) 0.022   0.015
H (41) 0.032   0.021
H (42) 0.039   0.027
H (43) 0.026   0.017
H (44) 0.029   0.019
H (45) 0.001   0.001
H (46) -0.003   0.000
H (47) 0.003   0.001
H (48) 0.001   0.001
H (49) 0.001   0.001
H (50) 0.001   0.001
H (51) 0.001   0.000
H (52) 0.001   0.001
H (53) 0.001   0.000
H (54) 0.000   0.000
H (55) 0.002   0.001
H (56) 0.000   0.000

Fukui Indices (FIs)

Herein the electronic charges were calculated from the condensed Fukui functions, defined as the first order derivative of electron density of $\rho(\vec{r})$, with respect to 'N' number of electrons at steady external potential of $v(\vec{r})$ as follows:

$$f_k = \left(\frac{\partial \rho(\vec{r})}{\partial N}\right)_{v(\vec{r})} \tag{1}$$

For the susceptible nucleophilic attack ($\square\square^+$) and electrophilic attack ($\square\square^-$) the corresponding FIs are denoted separately by the following equations [37]:

$$f_k^+ = q_k(N + 1) - q_k(N) \tag{2}$$

$$f_k^- = q_k(N) - q_k(N - 1) \tag{3}$$

Herein, $q_k(N)$ is associated with the gross charge of kth atom, whilst $q_k(N)$, $q_k(N + 1)$ and $q_k(N - 1)$ represents the neutral, negatively charged and positively charged entities Hirshfeld and Mulliken population analysis-based Fukui functions that have been derived by the finite difference approximation.

Application in Smartphone based colorimetric sensory prototype

Components of the prototype. The overall set up of the sensory prototype comprises of the indigenously fabricated light weight black acrylic make prototype box which consists of a compartment on one side wherein the Smartphone readily slides in. The other end consists of a circular sample holder with black lid for placing the vial containing the sample solution and covering the same to avoid false positive signals owing to penetration of any external light. 1 sheeld is basically one type of Arduino shield which is being used as a user interface to establish communication between the Smartphone and microcontroller. Turning on of any of the three LEDs (yellow, green or red) that are externally connected

with the 1 sheeld would provide the resulting output of the chemical response. Additionally, a power bank has been combined to provide the requisite power supply. The overview and segment wise visualization of the fabricated Smartphone assisted sensory prototype along with its AutoCAD diagram (SOLIDWORKS Software) has been provided in Fig. 9 and Fig. S24-S29†.
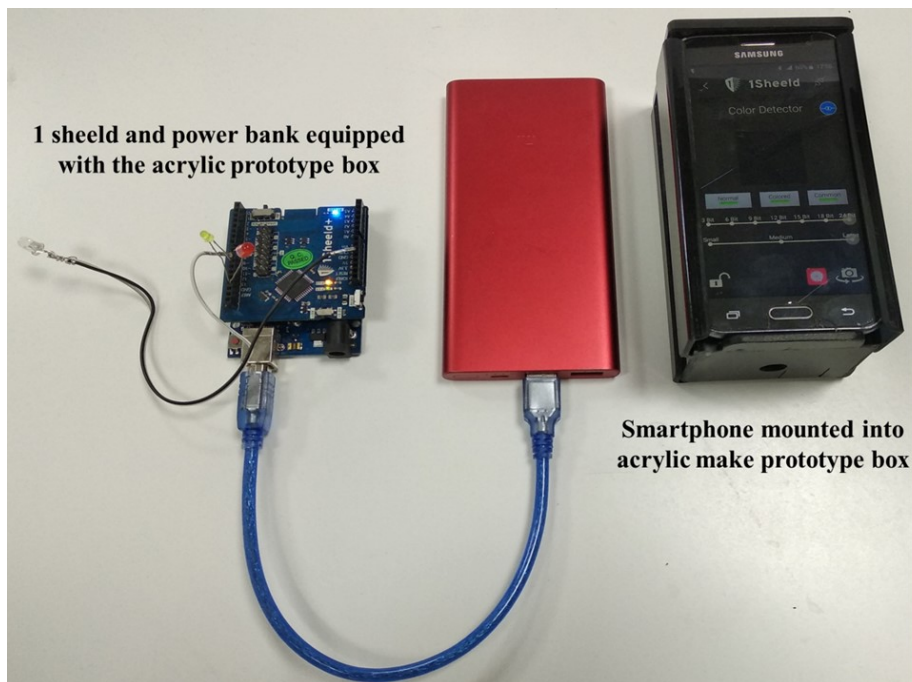
Fig. S24 An overview of the primary components of the Smartphone based prototype: smartphone, 1 sheeld and power bank.

Fig. S25 Sensory prototype displaying the Smartphone, black acrylic prototype box along with its lid separately.
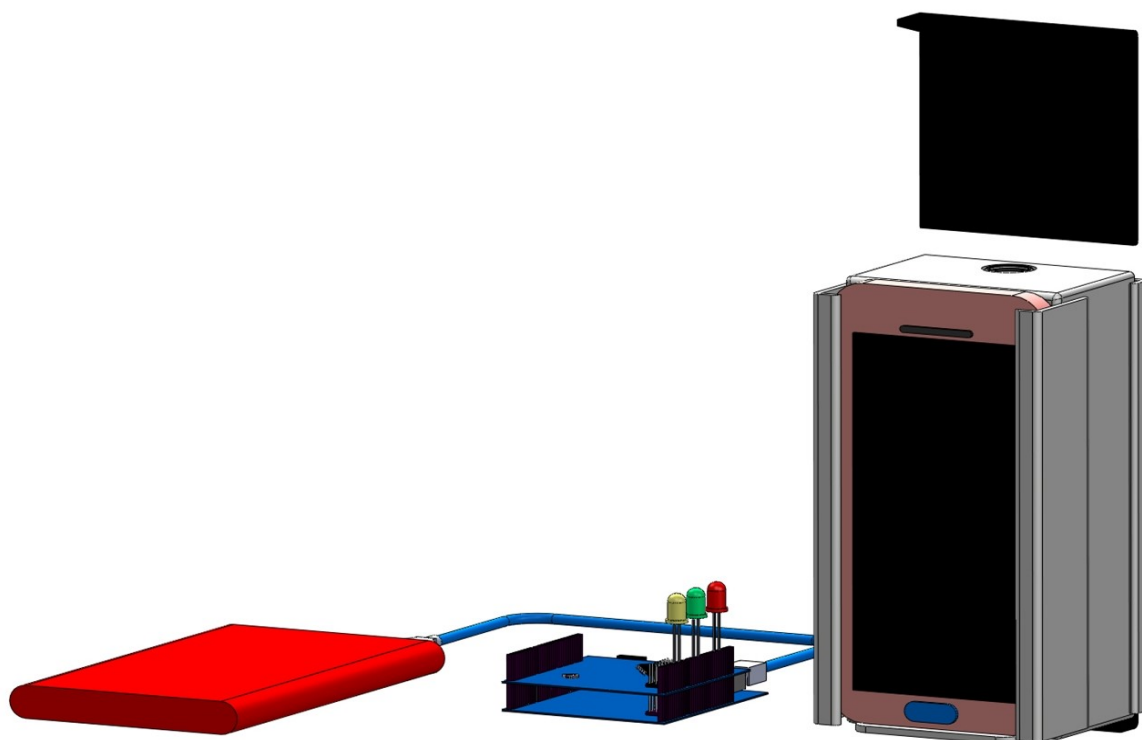
Fig. S26 AutoCAD diagram displaying the front view of the Smartphone based prototype.

Sample vial containing DNMH
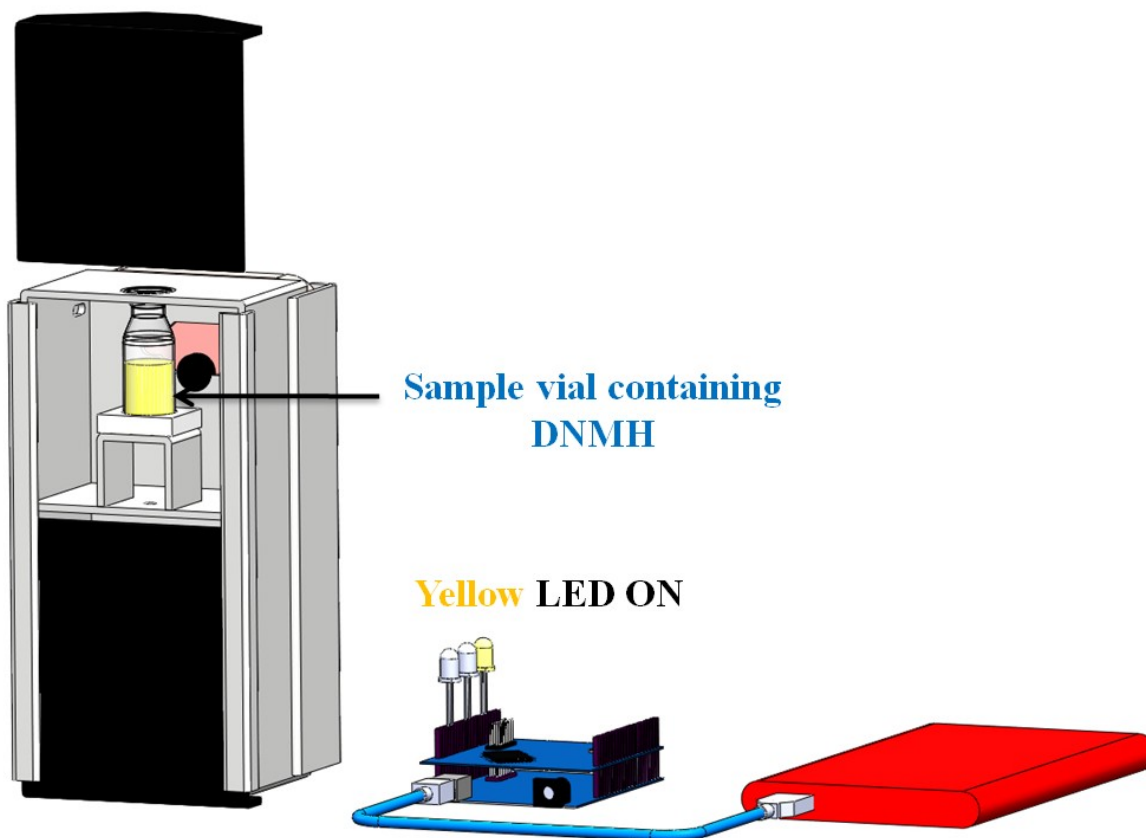
Yellow LED ON

Fig. S27 AutoCAD diagram displaying the output response as "**Yellow LED**" turned on when only **DNMH** solution (yellow colour) is present in the sample vial.
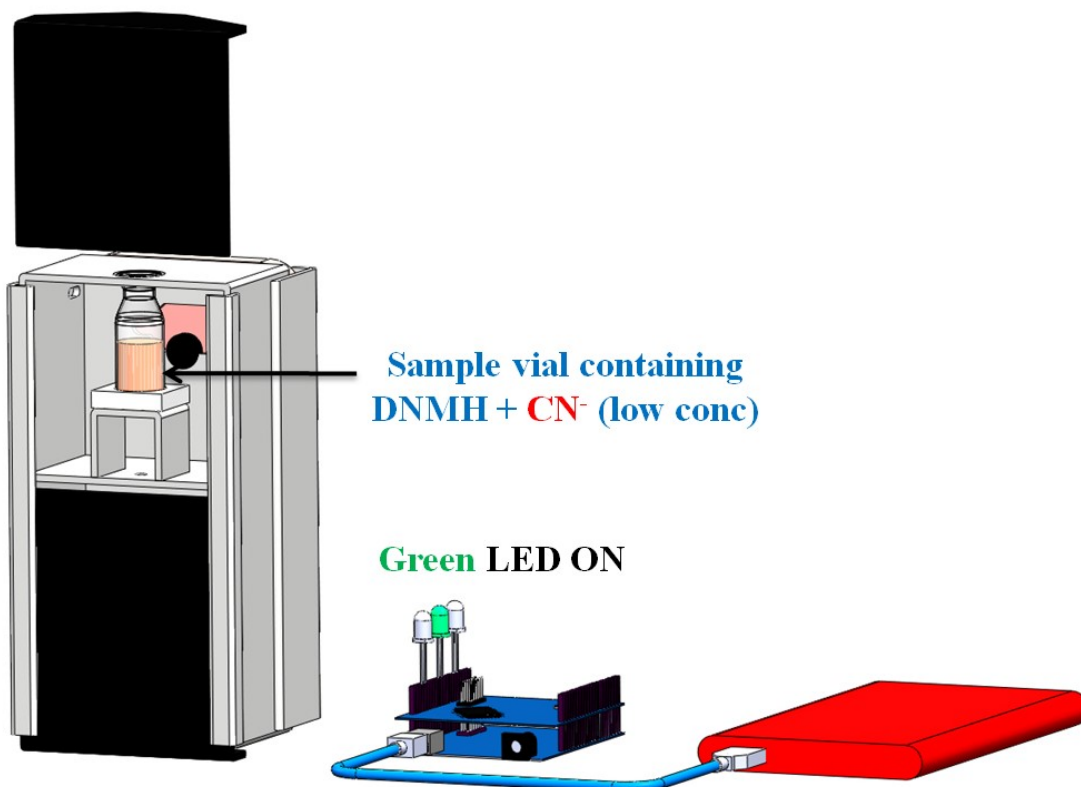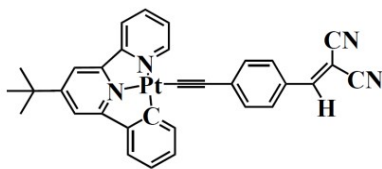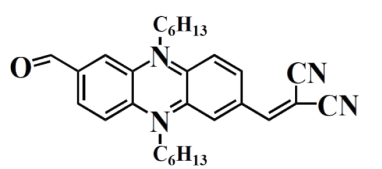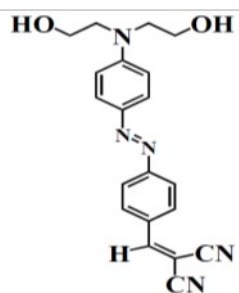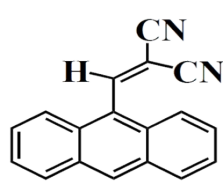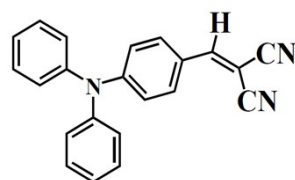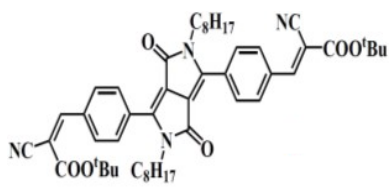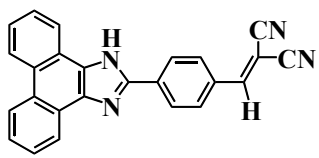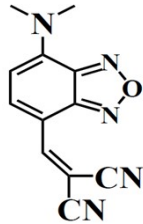
Fig. S28 AutoCAD diagram displaying the output response as "**Green LED**" turned on when **DNMH•••CN⁻** (low conc) solution (orangish red colour) is present in the sample vial.
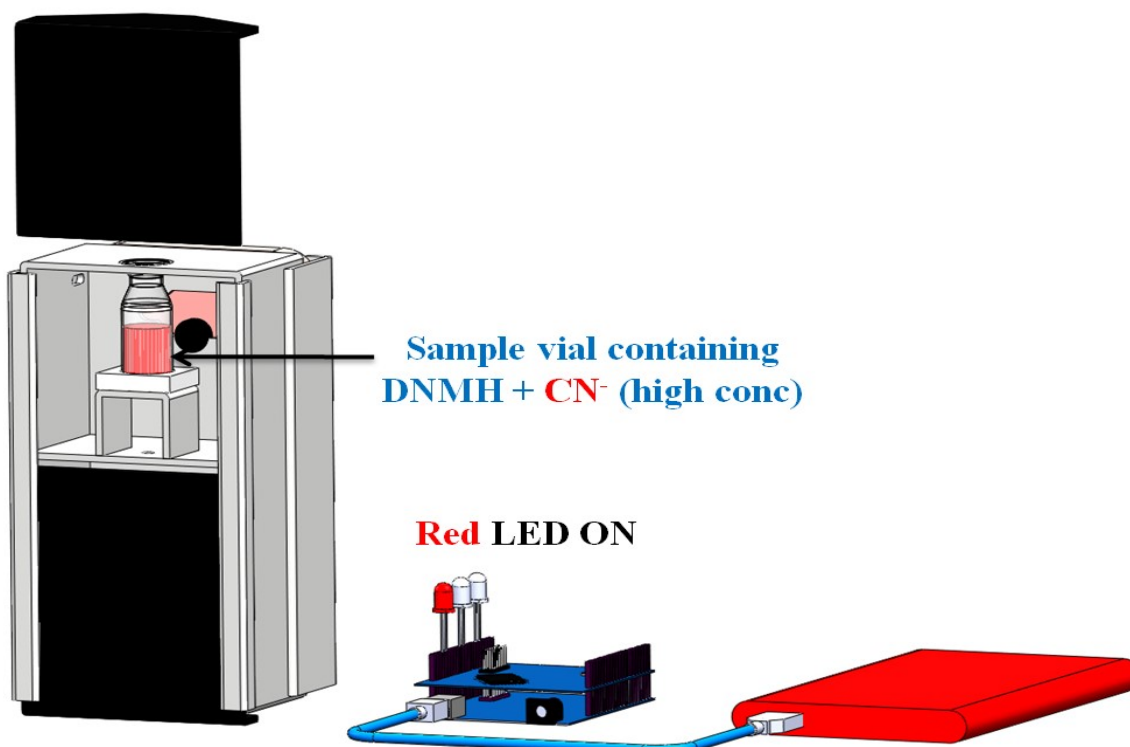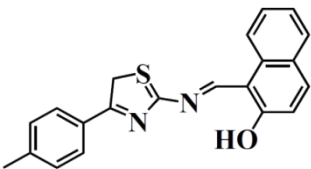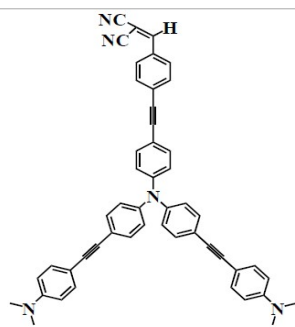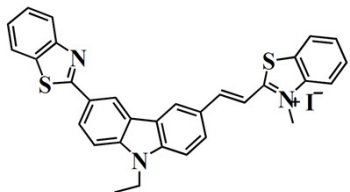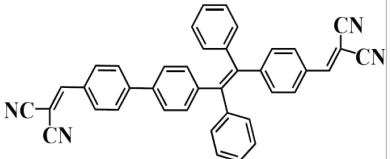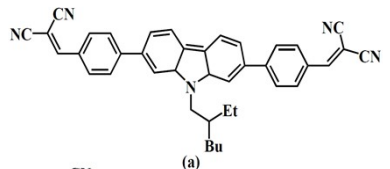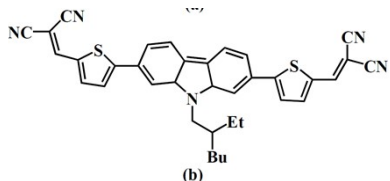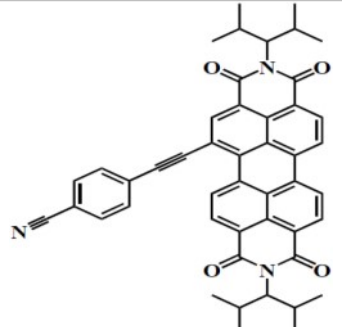

Fig. S29 AutoCAD diagram displaying the output response as "**Red LED**" turned on when **DNMH•••CN⁻** (high conc) solution (red colour) is present in the sample vial.
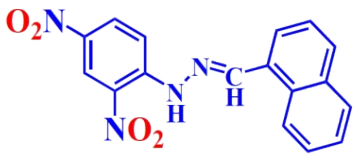
Table S17. Comparative literature survey of **DNMH** with the reported chemosensor for CN⁻ detection

Sl. no	Structure of the molecular probes	Detection Limit (M)	Binding Constant	Logic gate	Electro-chemical	Smartphone based	Ref.

			(M^{-1})		sensing	detection	
1.		8×10^{-7}	--	No	No	No	[4a]
2.		2.31×10^{-8}	6.692×10^4	No	No	No	[4b]
3.		1.1×10^{-6}	3.25×10^5	No	No	No	[4c]
4.		1.47×10^{-6}	--	No	No	No	[4d]
5.		9.8×10^{-9}	--	No	No	No	[4e]
6.		7.5×10^{-7}	--	No	No	No	[4f]
7.		1.26×10^{-6}	--	No	No	No	[4g]
8.		1.47×10^{-6}	--	No	No	No	[4h]

9.		19.4×10^{-6}	2.2×10^{3}	No	No	No	[4i]
10.		6.8×10^{-7}	--	No	No	No	[4j]
11.		9×10^{-8}	--	No	No	No	[4k]
12.		2×10^{-7}	--	No	No	No	[4l]
13.		1.26×10^{-7} 1.4×10^{-7}	--	No	No	No	[4m]
14.		$1\text{-}10\times10^{6}$	--	Yes	Yes	No	[4n]

15.	 **(DNMH)**	**298 nM**	**4.48×10^6 M^{-1}**	**Yes**	**Yes**	**Yes**	**This work**

References

[1] S. Mai, B. Ashwood, P. Marquet, C. E. Crespo-Herna´ndez, L. Gonza´lez, *J. Phys. Chem. B*., 2017, **121**, 5187-5196.

[2] Proceedings of the National Academy of Sciences, 2008, 105 (36), 13235-13240, DOI: 10.1073/pnas.0801025105.

[3] P. Ghosh, A. Hazra, M. Ghosh, N. C. Murmu, P. Banerjee, *J. Mol. Struct.*, 2018, **1157**, 444-449.

[4] (a) J.-L. Fillaut, H. Akdas-Kilig, E. Dean, C. Latouche and A. Boucekkine, *Inorg. Chem*., 2013, **52**, 4890-4897.

(b) L. Yang, X. Li, J. Yang, Y. Qu and J. Hua, *ACS Appl. Mater. Interfaces.*, 2013, **5**, 1317-1326.

(c) X. Cheng, Y. Zhou, J. Qin and Z. Li, *ACS Appl. Mater. Interfaces.*, 2012, **4**, 2133-2138.

(d) M. Shahid and A. Misra, *Anal. Methods*., 2013, **5**, 434-437.

(e) X. Yang, X. Chen, X. Lu, C. Yan, Y. Xu, X. Hang, J. Qu, R. Liu, *J. Mater. Chem. C*., 2016, **4**, 383-390.

(f) L. Wang, L. Zhu, D. Cao, *New J. Chem*., 2015, **39 (9)**, 7211-7218.

(g) L. Long, L. Zhou, L. Wang, S. Meng, A. Gong, F. Du, C. Zhang, *Anal. Methods*., 2013, **5**, 6605-6610.

(h) Z. Liu, X. Wang, Z. Yang and W. He, *J. Org. Chem*., 2011, **76**, 10286-10290.

(i) S. M. Kim, M. Kang, I. Choi, J. J. Lee and C. Kim, *New J. Chem*., 2016, **40**, 7768-7778.

(j) E. Thanayupong, K. Suttisintong, M. Sukawattanasinitt and N. Niamnont, *New J. Chem*., 2017, 41**(10)**, 4058-4064.

(k) X. Sun, Y. Yang, X. Deng, J. Zhang and Z. Zhang, *RSC Adv*., 2016, **6**, 10266-10271.

(l) Y. Zhang, D. Li, Y. Li and J. Yu, *Chem. Sci*., 2014, **5**, 2710-2716.

(m) R. K. Konidena and K. R. J. Thomas, *RSC Adv*., 2014, **4**, 22902-22910.

(n) M. A. Kaloo, R. Mishra and J. Sankar, *J. Mater. Chem. C*., 2015, **3 (8)**, 1640-1644.